Ordering of Octahedral Vacancies in Transition Aluminas

Wang, Yuan Go; Bronsveld, Paul M.; Hosson, Jeff Th.M. De; Djuričić, Boro; McGarry, David; Pickering, Stephen

Published in:
Journal of the European Ceramic Society

Publication date:
1998

journal

J. Am. Ceram. Soc., **81** [6] 1655–60 (1998)

Ordering of Octahedral Vacancies in Transition Aluminas

Yuan Go Wang, Paul M. Bronsveld,* and Jeff Th. M. DeHosson*,†

Department of Applied Physics, Materials Science Centre, University of Groningen, Groningen 9747 AG, The Netherlands

Boro Djuričić,‡ David McGarry, and Stephen Pickering

Institute for Advanced Materials, Petten 1755 ZG, The Netherlands

The microstructure of transition aluminas obtained via the dehydration of boehmite has been characterized by using transmission electron microscopy (TEM). The presence of γ-, δ-, and θ-aluminas was identified by using selected-area electron diffraction. Modifications that resulted from the reordering of aluminum vacancies on octahedral sites in a cubic close-packed oxygen network have been detected and analyzed by using high-resolution transmission electron microscopy (HRTEM) combined with image simulations. A good correspondence of the observed and calculated images confirmed the ordering of vacant octahedral sites located on {011} and {01$\bar{1}$} planes that formed a zigzag configuration along the ⟨010⟩ direction. Two more arrangements of empty octahedral sites, but now concentrated on {001} planes, have been determined in the sintered powder-gel agglomerates. Structure analysis suggested that the modifications are all associated with the rearrangement of vacant sites during the phase transformation from γ-alumina to δ-alumina, and further to θ-alumina, and may be driven by configuration entropy minimization.

I. Introduction

TRANSITION aluminas obtained via the dehydration of boehmite (γ-AlOOH) have been the subject of attention, mainly because of their potential application as catalysts and/or carriers for catalysts. The dehydration of γ-AlOOH at high temperature (~1200°C) does not immediately result in the formation of corundum (α-Al_2O_3), the thermodynamically stable structure. Many metastable oxides, such as γ-, δ-, and θ-Al_2O_3, are produced as transition phases before conversion to α-Al_2O_3. The transformation sequence starting from boehmite is first γ, in the temperature range of 350°–700°C, then δ, between 800° and 1000°C, and subsequently θ, from 1000° to 1200°C, with a topotactic orientation being maintained throughout.[1,2] Although these transition aluminas have been detected for many years, single-crystal X-ray techniques could not be used to study their structures, because the grain size does not exceed 300 nm in most cases; therefore, it is difficult to identify the detailed structure unambiguously. Based on those reports, these transition aluminas all have deformed cubic close packing of the oxygen anions; thus, structurally, the differences between them involve only the arrangement of cations in an approximately cubic-packed oxygen network. γ-AlOOH has an orthorhombic structure, γ-Al_2O_3 has a tetragonal deformed spinel structure, δ-Al_2O_3 can best be described by a superstructure of γ-Al_2O_3 with the ***c***-axis tripled because of ordering of cationic vacancies on octahedral sites governed by a screw tetrad parallel to the *c*-direction, θ-Al_2O_3 forms a monoclinic phase, and α-Al_2O_3 is rhombohedral. Table I summarizes these relevant structural data. The transformation between these phases can be considered as a rearrangement of aluminum ions, accompanied by an exchange of vacant octahedral and tetrahedral sites, which may cause complex structural modifications.

The purpose of the present study is to reveal the ordering behavior of the vacant octahedral sites during the transformation from γ- to δ-Al_2O_3, and further to θ-Al_2O_3, using high-resolution transmission electron microscopy (HRTEM) combined with image simulation. It is part of a larger project in which homogeneous precipitation from metal salts is used to prepare nano-nanocomposites. For example, the presence of ceria (CeO_2) influences the phase transformation of the catalytic active γ-Al_2O_3, which limits the crystal size to <10 nm.[3,4]

II. Experimental Procedure

Alumina (Al_2O_3) powder was produced from γ-AlOOH that was dehydrated at 1200°C for 3 h. The powder was one sample out of two batches of five samples that were heat treated at different temperatures that were chosen in the above-mentioned crucial temperature regions. One batch was based on the addition of cerium salt, and the other—the one under study—was based on the addition of barium salt. The Al_2O_3 concentration was $2 \times 10^{-2}M$, and an amount of metal equivalent to 10 mol% CeO_2 or baria (BaO) in Al_2O_3 was used. A powder X-ray diffraction (XRD) scan showed the coexistence of δ-Al_2O_3, θ-Al_2O_3, and $BaO \cdot Al_2O_3$. The powder was dispersed in absolute alcohol using an ultrasonic agitator and placed on a carbon film that was supported by a copper grid. HRTEM was performed to examine the microstructure at the atomic level. A transmission electron microscopy (TEM) microscope (Model 4000EX/II, JEOL, Tokyo, Japan) equipped with a top-entry goniometer stage with tilt angles up to 30° in the *x* and *y* directions was used at 400 kV, which revealed the detailed structure of the transition aluminas. High-resolution micrographs were recorded under symmetrically incident conditions, to correspond with the image simulations. The direct magnification on the micrographs was 500 k×. The exposure time was chosen to be as short as possible, usually <2 s, to avoid specimen drift due to mechanical and electrical instability. Crystals with ⟨100⟩ orientations were selected so that the images always included the {001} plane, which makes it easy to identify the arrangement of aluminum vacancies along the ⟨001⟩ direction. Large-angle-tilt electron diffraction and energy-dispersive X-ray analysis were conducted using a TEM

T. E. Mitchell—contributing editor

Manuscript No. 191093. Received April 10, 1997; approved October 6, 1997.

Author YGW acknowledges the support from The Netherlands Organisation for Scientific Research (NWO, The Hague, The Netherlands) and the Materials Science Centre of the University of Groningen.

*Member, American Ceramic Society.

†Author to whom correspondence should be addressed (E-mail address: hossonj@phys.rug.nl).

‡Currently with Hoogovens Research and Development, 1970 CA Ijmuiden, The Netherlands.

Table I. Crystal Data of Transition-Alumina Phases

Phase	Lattice parameters	Bravais lattice†
γ-AlOOH	$a = 0.370$ nm, $b = 1.223$ nm, $c = 0.287$ nm	Orthorhombic (*Amam*)
γ-Al_2O_3	$a = b = c = 0.790$ nm	Spinel (*Fd*3*m*)
δ-Al_2O_3	$a = b = 0.793$ nm, $c = 2.350$ nm	Tetragonal (*P*4*m*2)
θ-Al_2O_3	$a = 0.562$ nm, $b = 0.291$ nm, $c = 1.179$ nm, $\beta = 103.8°$	Monoclinic (*A*2/*m*)
α-Al_2O_3	$a = 0.476$ nm, $c = 1.299$ nm	Rhombohedral (*R*-3*c*)

†Term given in parentheses is the space group.

microscope (Model 200CX, JEOL) equipped with a side-entry goniometer stage and an energy-dispersive spectrometry (EDS) spectrometer (EDAX Instruments, Prairie View, IL).

Image simulations were performed by using the MacTempas multislice program.[5] The parameters of the microscope used in the simulation were as follows: the spherical aberration coefficient, C_s, was 1.0 mm; the beam divergence, α, was 0.50 mrad; the Gaussian defocus spread, Δ, was 5 nm; and the objective aperture, r, was 0.09 nm^{-1}.

III. Results

(1) Large-Angle-Tilt Electron Diffraction

Figure 1 is a bright-field TEM micrograph of a modified transition-alumina grain. It was chosen because of its typical zigzag structure in the HREM image; however, this structure should be considered to be a general phenomenon, because it occurred in 50% of the ~100 grains that were studied. The corresponding diffraction pattern was close to that of the δ-phase material; however, the morphology was different, because typical δ-phase material is similar in appearance to an elongated porous strip. EDS analysis proved the material to be free of barium. Figure 2(A) is an electron diffraction pattern with the electron beam incident along the [100] zone axis. It is distinguished from the reported δ-phase by the appearance of the forbidden reflections with Miller indices (0½0), (010), (002), etc.[1] The (0½0) superstructure reflection indicates a doubling of the lattice parameter along the ***b***-axis. Large-angle-tilt experiments were performed. Figures 2(B) and (C), obtained by tilting the sample around the (001) row in Fig. 2(A), are the related diffraction patterns, with the incident beam parallel to the [110] and [010] directions, respectively. Figure 2(C) is similar to Fig. 2(A), in that the same superstructure reflection (½00) can be observed, although it is very weak indeed. Based on the δ-Al_2O_3 cell parameters, the superstructure and forbidden reflections (½00), (0½0), (110), and (200) are observed. Initially, the new phase should have a tetragonal symmetry, with the ***a***- and ***b***-axes of the δ-Al_2O_3 structure doubled. However, by accepting this symmetry, one should expect the (½½0) superstructure reflection to be present in the diffraction pattern when the electron beam is parallel to the [110] zone axis; Fig. 2(B) shows that this is not the case. Therefore, the (½00) and (0½0) reflections both are not present in one grain at the same time. A very plausible explanation is that these superstructure reflections are produced by domains of the modified δ-Al_2O_3 structure with, alternatively, the corresponding ***a***- or ***b***-axis doubled. Such grains should show the (0½0) in the [100] electron diffraction pattern and the (½00) in the [010] pattern. Because the δ-phase has tetragonal symmetry, it is reasonable to believe that the ***a***- and ***b***-axes may be doubled equally when such a phase forms. These two grains relate to each other via a symmetric rotation around the [001] axis through 90° and result in a so-called 90° orientation variant.

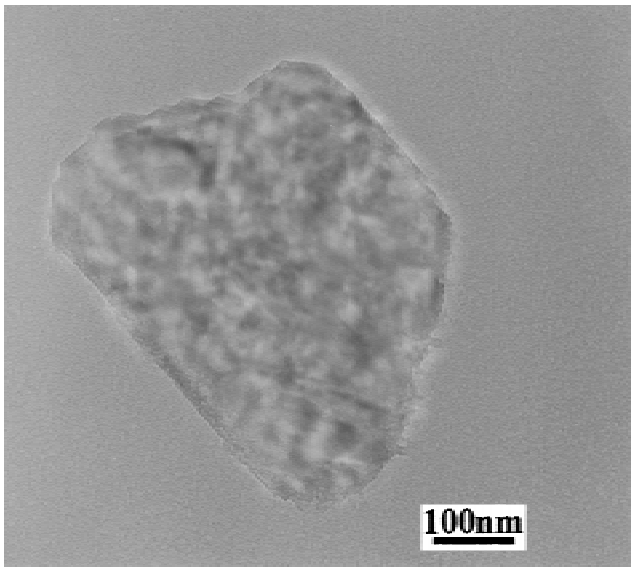

Fig. 1. Bright-field TEM micrograph showing the morphology of a modified transition-alumina grain.

The length of the ***c***-axis of this structure could be determined with the help of the following consideration. If the ***c***-axis would have remained the same during the transformation, the (111) reflection should have been present in Fig. 2(B). However, this situation does not seem to be the case. The calculated reflections coincide with the experimental ones only if one assumes that the ***c***-axis is reduced to half the original value. Therefore, the only consistent explanation of Figs. 2(A), (B), and (C) leads to the following cell constants: $a = 0.7943$ nm, $b = 1.5886$ nm, and $c = 1.175$ nm. Based on these parameters, the superstructure reflections can now be indexed with only integer Miller indices: (010), (001), (110), (111), and (100). There does not seem to be any limitation for the combinations (*hkl*), (*hk*0), (*h*00), (0*k*0), and (00*l*). Therefore, it can be concluded that the Bravias lattice is primitive and no screw and glide symmetries are present in this modified phase, which will be confirmed by high-resolution images, as given in the next section.

(2) High-Resolution Imaging and Simulation

Figure 3 shows one of the corresponding HRTEM images. Important features of this image include the strings of image dots, usually four dots separated by 0.28 nm, with enhanced contrast and lying alternately on the (011) and (01$\bar{1}$) planes of the deformed spinel structure or the (013) plane of the δ-phase. The strings appear in pairs and form a zigzag configuration along the [010] direction. These strings are apparently in the (010) mirror-related positions, and the periodicity of a unit of zigzag in the [010] direction equals double the length of the ***b***-axis. Such an assignment of image dots modulates the original crystal, and the periodicities of modulation are determined in the micrograph to be 1.59 and 1.18 nm, along the [010] and [001] directions, respectively. In the ⟨100⟩ projected spinel structure, channels surrounded by cations and anions are 0.28 nm apart in the ⟨011⟩ directions,[6] so that the image dots in Fig. 3 may correspond to these channel positions. In analogy with the similar structure of iron(III) oxide (Fe_2O_3),[7] the aluminum vacancies in the δ-phase are thought to be ordered on the octahedral positions of the spinel structure and, thus, the strings of brighter image dots should relate to the concentration of

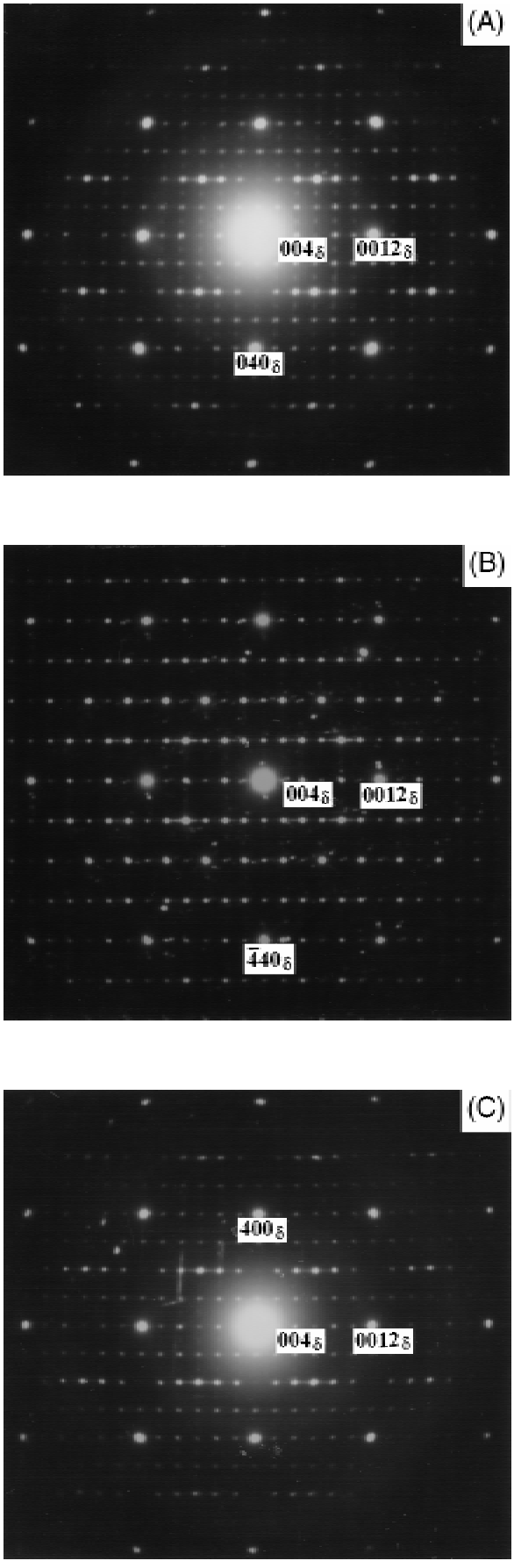

Fig. 2. Three low-index electron diffraction patterns of the grain in Fig. 1 obtained via large-angle tilt around the (001) row with incident electron beams parallel to (A) [100], (B) [110], and (C) [010].

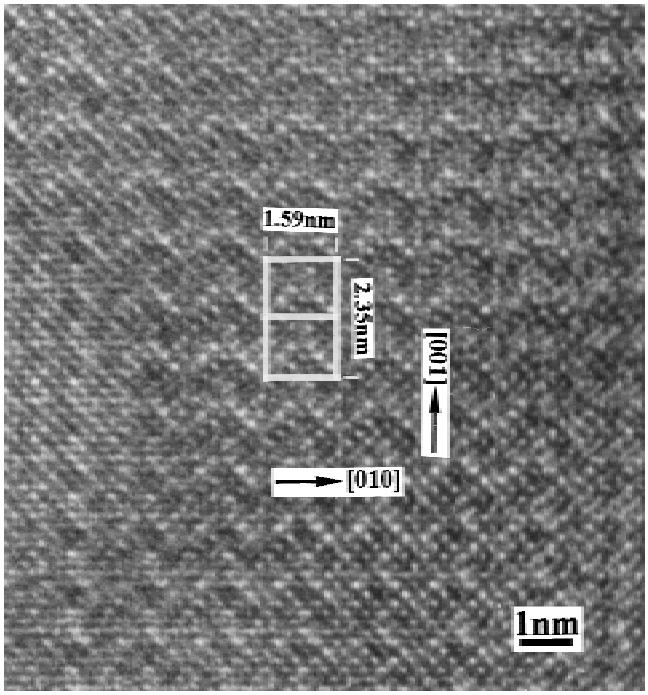

Fig. 3. [100] high-resolution image demonstrating vacancies located on the (011) and (01$\bar{1}$) planes, forming a characteristic zigzag configuration.

vacant octahedral sites on the (011) plane of the spinel or the (013) plane of the δ-phase. Structural analysis of the spinel-type γ-phase shows that a superstructure with $a = 0.7943$ nm, $b = 1.5886$ nm, and $c = 1.175$ nm cannot be introduced if only ordering of aluminum vacancies on the octahedral sites is considered. Therefore, the phase transformation must involve the rearrangement of aluminum cations. Keeping the oxygen network unchanged and rearranging aluminum ions in this network, a possible structure model is considered and displayed in Fig. 4(A). The structure consists of the alternate stacking of vacant octahedral sites, four empty octahedral positions arranged side by side on the (011) plane of the deformed spinel connected to a similar string of empty octahedral sites along the (01$\bar{1}$) plane to form a ''V''-shaped figure along the [010] direction. The aluminum cations located in the triangle separated by the ''V'' alter their positions by a ½ [100] shift and occupy these new octahedral and tetrahedral sites. Pairs of aluminum ions at ½ and ¾ height become neighbors across the ''V.'' The vacant octahedral sites that are ordered in such a way destroy the screw symmetry operations along the [001] direction in the δ-phase. Each unit cell contains a total of eight cationic vacancies, which satisfies the stoichiometry of alumina.

Image simulations were made for different thicknesses and defocus values, and the results are shown in Fig. 4(B). Images obtained at an underfocus of −55 nm reflect the channels of the spinel crystal. In this case, the channels with aluminum vacancies around them are resolved as giving spots that have bright contrast. The stronger contrast is caused by vacant octahedral sites around the channels and shows a good match with the observed high-resolution micrograph. The image calculated at an underfocus of −65 nm reflects the projected potential of the crystal. In this case, octahedral positions are imaged and irregular contrast appears at the vacant octahedral sites. The coincidence of simulated contrast with experimental results confirms the suggested structure model.

(3) Aluminium Vacancies Ordered on the (001) Plane

The coexistence of many grains that are often intergrown on a nanometer scale and with different arrangements of vacant

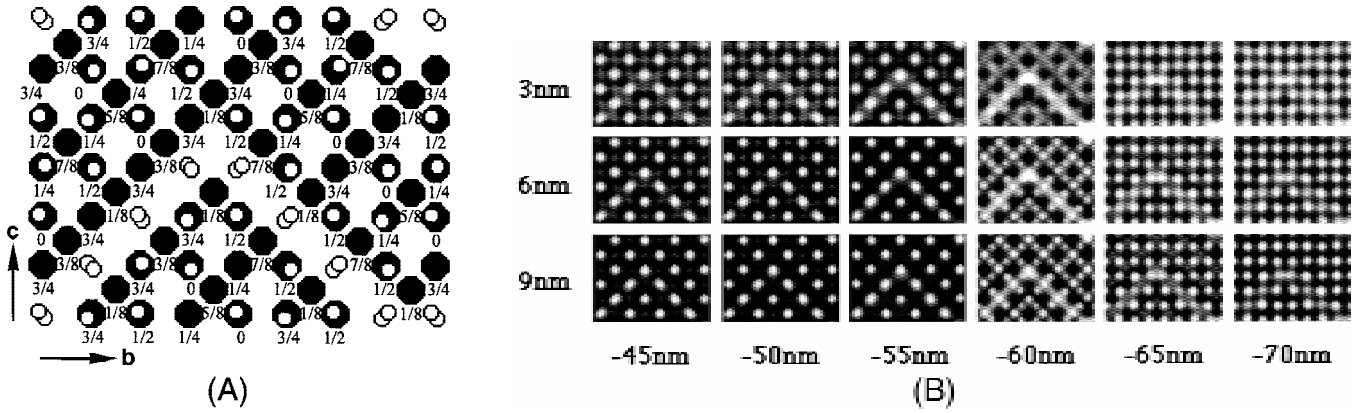

Fig. 4. (A) Structure model suggested for the modified transition alumina in Fig. 3 ((○) oxygen atoms and (●) aluminum atoms; numbers beneath the circles indicate the height of the atom along the [100] axis); some of the aluminum atoms have adjusted their position slightly. (B) Through-focus and through-thickness simulations calculated for the model; the image obtained at an underfocus of −55 nm produces the channels and the one obtained at −65 nm produces the octahedral sites (the empty octahedral site is clearly visible because of its brighter contrast).

octahedral sites, but belonging to the same stoichiometry of alumina, have been observed. Figure 5 shows another modified alumina. The characteristic of this figure is the periodic appearance of an isolated column of brighter image dots on the (001) plane. Such regular variations in image contrast due to the stacking sequence of the (001) planes represent a modulation wave in the host crystal with a wavelength of 1.18 nm along the [001] direction, which is half the length of the ***c***-axis of the δ-phase. In this image, the distance from dot to dot is 0.2 nm, which is equal to the distance between octahedral sites projected on the (100) plane. These image dots represent the octahedral sites that are known from the image simulation of Fig. 4(B). The irregular contrast of image dots results from the empty octahedral sites. Figure 6(A) suggests a proposed structure model that is in accordance with this assumption. In this model, four vacant octahedral sites are concentrated on one particular (001) plane and are separated by 1.18 nm from an identical (001) plane. A unit cell of spinel resides between these two layers. The unit-cell constants are $a = b = 0.7943$ nm and $c = 1.175$ nm. Such an arrangement of empty octahedral sites eliminates the symmetry operations of the δ-phase, and a twofold symmetry that passes through the tetrahedral position at the height of ⅛, instead of the screw tetrad along the [001] direction, is created. The possible space group derived from this model is $P2$. Figure 6(B) shows the calculated images. The images obtained at a thickness of 3 nm with an underfocus of −65 nm matches well with the experimental micrograph. The diffraction pattern for this model has been calculated. The superlattice reflections appear between the main reflections of the δ-phase along the [001] direction.

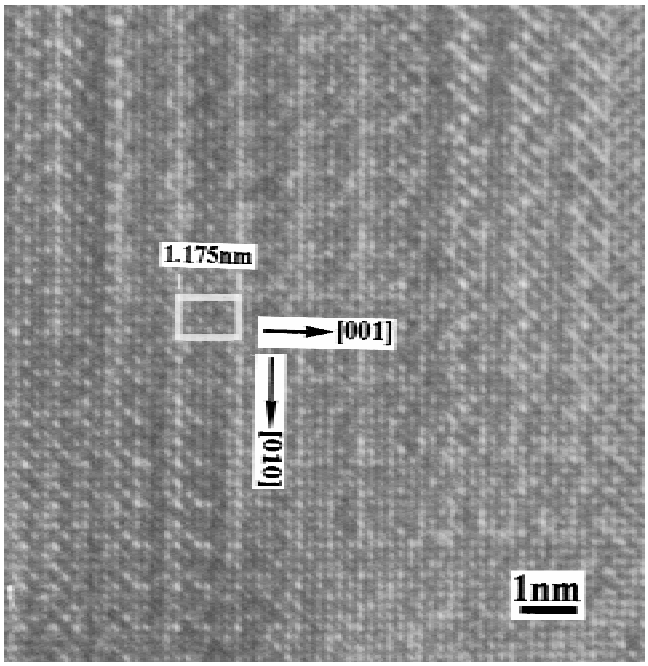

Fig. 5. [100] high-resolution image illustrating another modified transition alumina. Isolated (001) layers with brighter contrast can be found arranged with a repeat distance of 1.175 nm.

Figure 7 shows yet another high-resolution image taken of the same sample as that used in Fig. 5. The major feature, based on the difference in contrast of the image dots in this micrograph, is similar to those in Fig. 5, the only difference being an extra contrast with a periodicity of 0.59 nm along the [001] direction, which is half the periodicity of the modulation wave in Fig. 5. Careful analysis on the spinel structure shows that it is impossible to introduce a superstructure with a periodicity of 0.59 nm along the ⟨001⟩ directions. The actual periodicity of the modulation wave in Fig. 7 should be 1.18 nm. The contrast variation have been proven to result from the presence of empty octahedral sites. A possible arrangement of aluminum vacancies is proposed and shown in Fig. 8(A). In this case, four empty octahedral sites are divided into two groups and are arranged on alternative (001) planes that are separated by 0.59 nm along the [010] direction. Aluminum cations have also adjusted their positions, and the periodicity in the [001] direction is 1.18 nm, which is double the periodicity that appears in the high-resolution image. Three screw operations can be found along the cell axes: a 2_1 screw operation passes through empty octahedral sites along the [100] direction, another 2_1 screw operation also passes through empty octahedral sites at the height of ⅛ along the [001] direction, and a third 2_1 screw operation appears midway between two (001) planes with empty octahedral sites at the height of ⅝ along the [010] direction. The space group for this modified alumina is suggested to be $P2_12_12_1$. Figure 8(B) shows the simulated images. The image obtained at a thickness of 5 nm with an underfocus of −65 nm shows the periodic change in contrast at the (001) planes with empty octahedral sites, and the change matches well with the observed change.

IV. Discussion

An early study in which the ordering of cationic vacancies was already mentioned has been made on the $MgO{\cdot}nAl_2O_3$ system.[8] For $n = 1$, we have the normal spinel structure $A[B_2]O_4$, with eight magnesium atoms at the eight tetrahedral positions and sixteen aluminum atoms at the sixteen octahedral

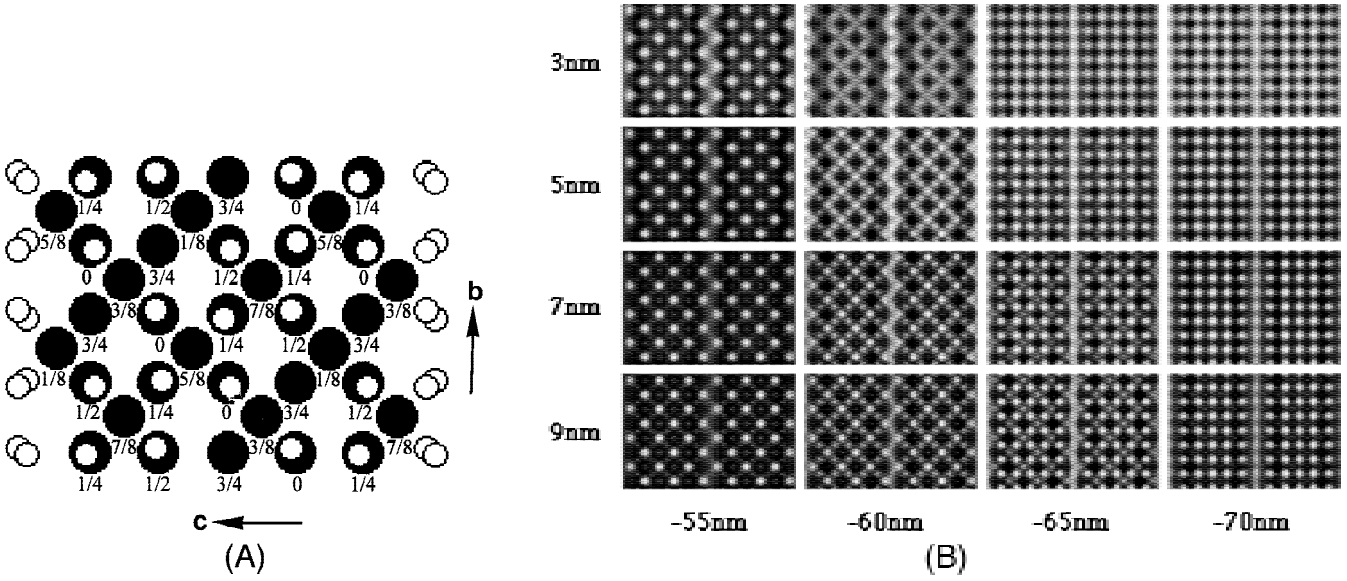

Fig. 6. (A) Proposed structure model for the modified transition alumina in Fig. 5; the vacant octahedral sites are all concentrated on the (001) plane. A perfect spinel cell is located between two empty octahedral layers. (The circles and numbers have the same meaning as those in Fig. 4.) (B) Simulated images for different thicknesses and underfocus values; the image obtained at a thickness of 3 nm and defocus of −65 nm shows the strongest contrast variation. Four unit cells are given.

positions. In this respect, γ-Al_2O_3 is a defect spinel with formula $B_{8/3}O_4$. Because there are fewer aluminum ions than needed to adopt the perfect spinel structure, they are rearranged over the available sites to give an almost-tetragonal unit cell with an inherent number of vacant sites, bringing with it a type of metastable character. A more recent study comes close to our original goal; it attempted to describe the influence of BaO on the stability of transition alumina.[9] However, in the area where we studied these vacancy-ordered transition aluminas, we could not find any traces of barium. Moreover, very similar intermediate phases were reported recently in nondoped Al_2O_3.[10,11] The first observation was made in material manufactured via electrohydrodynamic atomization, and the other observation was made in material produced from the melt. Both groups used convergent-beam electron diffraction to identify the structure of grains that were only tens of nanometers in size. In both cases, the lattice parameters were measured as ($2a_\gamma$, $1.5a_\gamma$, a_γ). The original γ-AlOOH sequence does produce a δ-Al_2O_3 with lattice parameters (a_γ, a_γ, $3a_\gamma$), as was reported by Lippens and De Boer.[1] This was also our starting point; however, we now know that this former phase may also appear on the γ-AlOOH sequence and for good reasons. A possible space group determination would be $P2$, which is not confirmed by the two convergent-beam determinations, of which one proposes $P2_12_12_1$ and the other suggests *Pmma*. In this most recent article, the presence of magnesium established the spinel structure even more. The transition-alumina phase with lattice parameters $a = b = 0.56$ nm and $c = 2.37$ nm reported by Repelin and Husson[12] was not observed in this investigation.

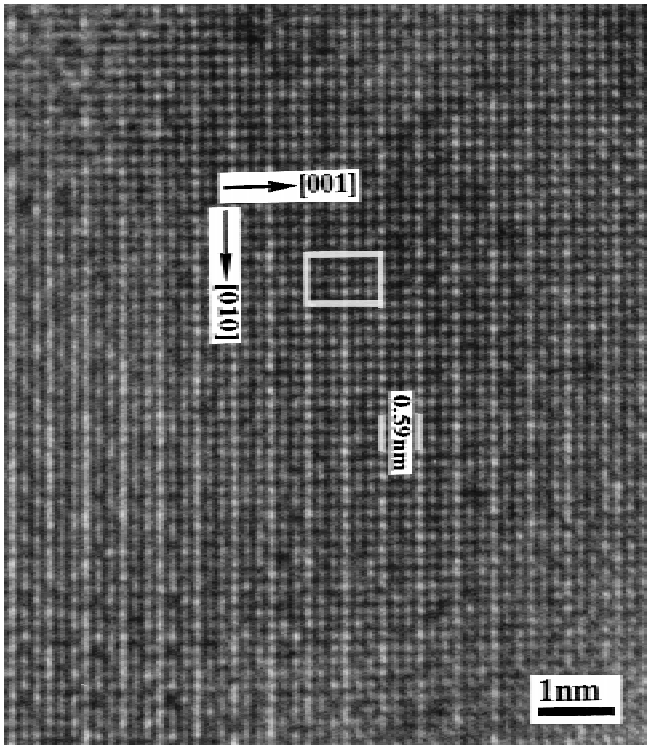

Fig. 7. [100] high-resolution micrograph showing contrast variation with a repeat distance of 0.59 nm along the [001] direction.

It seems that the important characteristic of the ordering of cationic vacancies in these modified alumina phases is the reassignment of the ***c***-axis to half that which belongs to the δ-phase. The common (001) interplanar distance of these modified phases is beneficial for further transformation to the θ-phase. Moreover, the distribution of vacant octahedral sites is no longer via the screw tetrad, which was lost during the reordering process; the distribution results in a change in space group, from tetragonal to orthorhombic and further to monoclinic.

A final point is the driving force for the vacant sites to be ordered. Ordering of vacancies is a frequently occurring phenomenon in alloys, ceramics, and natural minerals. A good example is pyrrhotite ($Fe_{1-x}S$). Iron vacancies that are ordered in different configurations in pyrrhotite have been observed to form many superstructures.[13] Calculations have shown that iron vacancies should always be ordered, to keep the energy of the crystal (mainly entropy) at a relatively low level.[14] Therefore, the driving force for the ordering of aluminum vacancies in these modified phases may be the configuration entropy, which stabilizes these structures. In a rather interesting paper based on neutron diffraction data, Zhou and Snyder[15] made the point (although they do not even mention the δ-phase) that the

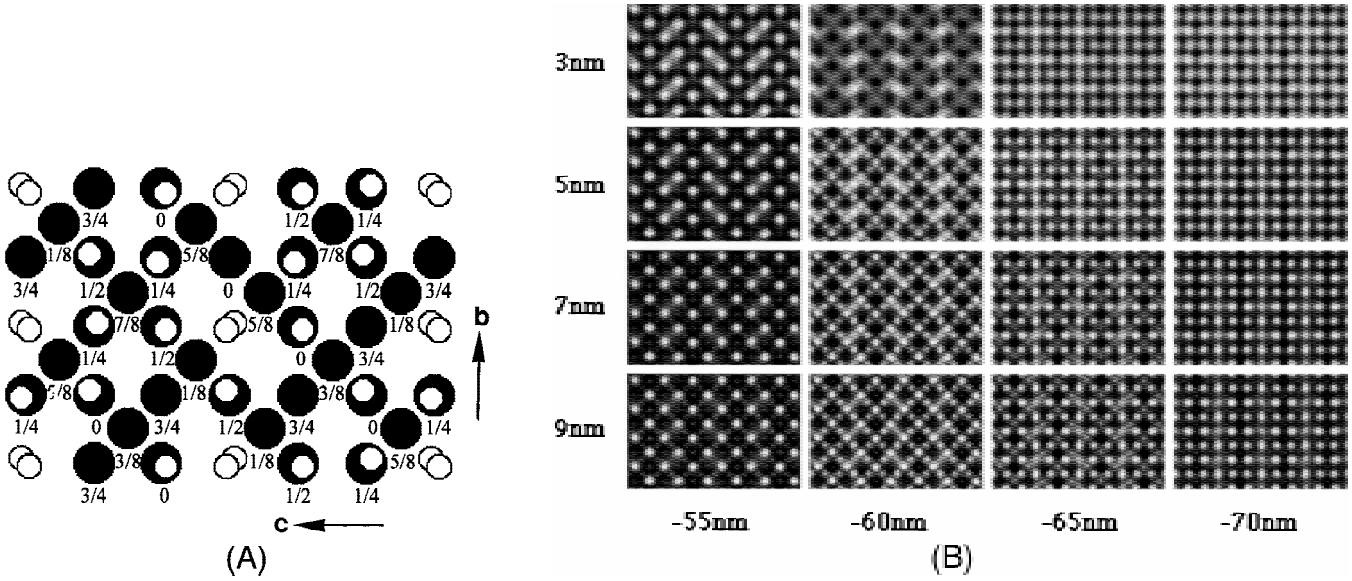

Fig. 8. (A) Structure model suggested for the modified transition alumina in Fig. 7; rearrangement of aluminum has been made in this model. (The circles and numbers have the same meaning as those in Fig. 4.) (B) Simulated images for different thicknesses and underfocus values. The images at a defocus of −65 nm show a good correspondence with the experimental results.

Table II. Crystal Data of Modified Transition-Alumina Phases

Phase	Lattice parameters (nm)			Bravais lattice†	Plane of vacancies
	a	*b*	*c*		
Mod-I	0.794	1.589	1.175	Orthorhombic (*P*2)	(011) and (01$\bar{1}$)
Mod-II	0.794	0.794	1.175	Orthorhombic (*P*2)	(001)
Mod-III	0.794	0.794	1.175	Orthorhombic ($P2_12_12_1$)	(001)

†Term given in parentheses is the space group.

transition from γ-Al_2O_3 to θ-Al_2O_3 is a displacive rather than reconstructive recrystallization process.

V. Conclusion

Three modified transition aluminas have been suggested (Table II). The vacant aluminum sites are proven to be located only on octahedral coordinated sites. No vacant sites have been found to be located on tetrahedral coordinated sites, which implies that these modified phases are closer to the δ-phase than to the θ-phase. The cationic vacant sites are concentrated on planes with low indices, such as {011} and {001}. The reordering destroys the screw tetrad in the δ-phase and introduces a phase transformation from tetragonal to orthorhombic and further to monoclinic; 90° orientation variants can be introduced during the rearrangement of cations.

References

[1]B. C. Lippens and J. H. De Boer, ''Study of Phase Transformations during Calcination of Aluminum Hydroxides by Selected Area Electron Diffraction,'' *Acta Crystallogr.*, **17**, 1312–21 (1964).

[2]S. J. Wilson and J. D. C. McConnell, ''A Kinetic Study of the System γ-AlOOH/Al_2O_3,'' *J. Solid State Chem.*, **34**, 315–22 (1980).

[3]K. J. Morrissey, K. K. Czanderna, R. P. Merrill, and C. B. Carter, ''Transition Alumina Structures Studied by HREM,'' *Ultramicroscopy*, **18**, 379–85 (1985).

[4]B. Djuričić, S. Pickering, and D. McGarry, ''Preparation and Properties of Alumina–Ceria and Alumina–Baria Nano-nano Composites,'' submitted to *J. Mater. Sci.*

[5]R. Kilaas, ''Defect Modeling in HRTEM Image Simulation''; pp. 528–29 in *Proceedings of the 49th Annual Meeting of the Electron Microscopy Society of America*. Edited by G. W. Bailey and E. L. Hall. San Francisco Press, San Francisco, CA, 1991.

[6]Y. G. Wang, D. H. Ping, and J. G. Guo, ''High-Resolution Transmission-Electron-Microscopy Observation of the Ultra-Fine Structure of Natural Magnetite,'' *J. Appl. Crystallogr.*, **27**, 96–102 (1994).

[7]C. Haas, ''Phase Transitions in Crystals with the Spinel Structure,'' *J. Phys. Chem. Solids*, **26**, 1225–31 (1965).

[8]N. Doukhan, J. C. Doukhan, and B. Escaig, ''TEM Study of High Temperature Precipitation in $(Al_2O_3)_n$·MgO Spinels,'' *Mater. Res. Bull.*, **11**, 125–34 (1976).

[9]N. Iyi, S. Takekawa, Y. Bando, and S. Kimura, ''Electron Microscopic Study of Barium Hexa-aluminates,'' *J. Solid State Chem.*, **47**, 34 (1983).

[10]V. Jayaram and C. G. Levi, ''The Structure of δ-Alumina Evolved from the Melt and the γ → δ Transformation,'' *Acta Metall. Mater.*, **37**, 569–78 (1989).

[11]S. Wang and H. J. Dudek, ''Structure of Phases in the δ-Al_2O_3 Fiber Studied by Convergent Beam Electron Diffraction,'' *Metall. Mater. Trans.*, **27A**, 3318–22 (1996).

[12]Y. Repelin and E. Husson, ''Etudes Structurales d'Alumines de Transition: l'Alumines Gamma et Delta'' (Structural Studies of Transition Aluminas: γ- and δ-Alumina), *Mater. Res. Bull.*, **25**, 611–21 (1990).

[13]H. Nakazawa and N. Morimoto, ''Phase Relations and Superstructures of Pyrrhotite,'' *Mater. Res. Bull.*, **6**, 345–58 (1971).

[14]E. F. Bertaut, ''Contribution à l'Etude des Structures Lacunaires: La Pyrrhotine,'' *Acta Crystallogr.*, **6**, 557–61 (1953).

[15]R.-S. Zhou and R. L. Synder, ''Structures and Transformation Mechanisms of the η, γ and θ Transition Aluminas,'' *Acta Crystallogr., Sect. B: Struct, Sci.*, **B47**, 617–30 (1991). □